Supplementary Appendix

Supplement to: Wang E, Mi X, Thompson MC, et al. Mechanisms of resistance to noncovalent Bruton's tyrosine kinase inhibitors. N Engl J Med 2022;386:735-43. DOI: 10.1056/NEJMoa2114110

This appendix has been provided by the authors to give readers additional information about the work.

SUPPLEMENTARY APPENDIX

Table of Contents

SUPPLEMENTARY METHODS

Mutational and copy number alteration analysis

MSK-IMPACT Heme/HemePACT variant calling of single nucleotide variants (SNVs), indels, and copy number alterations was performed as previously described.[1] Mutations are called based on paired analysis using the submitted patient-specific control samples (paired normal, non-malignant DNA from buccal swabs or fingernails) and an additional pooled, unmatched normal. This assay reports point mutations/SNVs, small indels (<30 bp in length), and larger insertions and deletions (<2,000 bp in length) in the protein-coding exons of the 576-gene panel (**Table 6** in the **Supplementary Appendix**) confirmed to be absent in the pooled, unmatched normal and somatic based on comparison of variant allele frequencies in the patient's tumor sample and matched buccal swabs or fingernails. MuTect (version 1.1.4) was used for SNV calling, and SomaticIndelDetector, a tool in GATK version 2.3.9 was used for detecting indel events. The following standard filters were applied to the raw MuTect and SomaticIndelDetector output as a first pass (with more rigorous filters being applied at a subsequent stage): variant frequency in tumor/variant frequency in normal >5x, number of mutant allele reads in tumor sample >5x, and variant frequency in tumor sample >1%. Variants were annotated using Annovar (version 527), and the output was reformatted using a custom script to ensure annotations of the cDNA, and protein primary sequence changes are compliant with HGVS standards. Dinucleotide and trinucleotide substitutions identified by the pipeline were annotated manually because this functionality was not supported by the version of Annovar used. Only variant annotations relative to the canonical transcript for each gene (derived from a list of known canonical transcripts obtained from the UCSC Genome Browser) were reported. In cases where variant calling was performed using an unmatched normal sample, variants with minor allele frequency >1% in the 1000 Genomes cohort were removed[2]. Further filtering for high-confidence SNVs and indel calls prior to the final step of manual review included the following: evidence in the literature for being an oncogenic or recurrent hotspot mutation; whether or not these were reproducible assay artifacts with occurrence of the variant in previously run pools of normal controls; technical characteristics (depth of coverage, number of mutant reads supporting the variant, and variant frequency); and whether or not the variant was exonic and non-synonymous.[2-4] Tumor mutational burden was calculated by dividing the number of non-synonymous mutations by the expected breadth of sequencing in the IMPACT Heme/HemePACT panel[1] (1.21 Mb). The cancer cell fraction (CCF) was calculated as

previously described.[5] In brief, the CCF for autosomal mutations was estimated to be two times the variant allele frequency (VAF) under the assumption that they are heterozygous. The cancer cell fraction (CCF) for X-linked mutations (e.g., BTK mutations) was estimated to be two times the VAF in females and equal to the VAF in males.

For copy number alteration analysis by IMPACT Heme/HemePACT, the criteria for gene amplification and deletions are as follows: if the fold change is greater than 2, it is reported as amplification. If the fold change is -2 or below, it is reported as a deletion. The degree of copy number change is influenced by tumor content and the ability to detect copy number changes is progressively compromised in samples with less than 50% tumor. For samples with low tumor content, the absence of detectable copy number changes should be interpreted with caution.

Genomic microarray DNA copy number and Copy-Neutral Loss of Heterozygosity (CN-LOH) analysis

Study patients with a diagnosis of CLL had DNA extracted from fresh peripheral blood, bone marrow, or lymph node (fresh flow cytometry single-cell suspension specimen or formalin-fixed paraffin-embedded tissue (FFPE)). Genomic single-nucleotide polymorphism (SNP) microarray tests were performed following the manufacturers' instructions. The SNP-array tests employed a CytoScan HD array (described previously[6]) and an OncoScan CNV assay chip with 220,000 SNP probes specifically covering about 900 cancer genes (both from Affymetrix/Thermo Fisher Scientific Inc., Santa Clara, CA). The CytoScan HD array contains 2.67 million probes consisting of probes detecting 750,000 unique SNPs and 1.9 million oligonucleotide probes, with a mean backbone spacing of one oligonucleotide probe every 2 kb and one oligonucleotide probe every 400 base pairs in targeted regions.[6] The mean spacing of SNP probes is 200 per megabase. All probes are 25 bp long. Each SNP is targeted by six probes, three for each allele. For CytoScan, the CEL files were converted to CYCHP files while for oncoscan, both CEL files from AT and CG products in combination were converted to an OSCHYP file. Data analysis was performed using ChAS software (version 3.2; Affymetrix) for cytoscan data and Oncoscan Nexus Express (Biodiscovery Inc., El Segundo, CA) for oncoscan data. All samples were manually reviewed and interpreted with a focus on recurring genomic abnormalities in CLL/SLL and other hematologic malignancies. The threshold genomic size to assess for gains or losses is approximately 400Kb. The threshold genomic size to assess for CN-LOH is approximately 10Mb.

Immunoglobulin Heavy Chain Gene (IGH) rearrangement study and IGH Variable Region (IGHV) somatic hypermutation assessment by next-generation sequencing

The variable (IGHV) and the joining (IGHJ) regions of the IGH locus are amplified by polymerase chain reaction (PCR) and are sequenced by next-generation sequencing (MiSeq) to determine the frequency, distribution, and specific sequence of each rearrangement (Lymphotrack IGH-Leader, InVivoScribe). The functionally rearranged sequence is compared to the germline sequences included in the IMGT (Immunogenetics) database for percent homology. A mutated status is assigned when the frequency of the mutation is 2% or greater. The sensitivity for a follow-up monitoring sample with a previously characterized clonal sequence is a clonal cell population of 0.5%.

Single-cell DNA sequencing analysis

Targeted single-cell DNA sequencing of cryopreserved peripheral blood mononuclear cells (PBMCs) collected pre-treatment and at on-treatment relapse from two patients with acquired BTK L528W mutations and resistance to pirtobrutinib was performed on a microfluidic, droplet-based platform developed by Mission Bio, as previously described[7] (the samples used are noted in **Table 1** in the **Supplementary Appendix**). Barcoded samples proceeded to PCR amplification using a customized Mission Bio CLL panel with 273 amplicons targeting 32 genes including BTK C481 and non-C481 mutations such as L528W. The identity and mutational profile of each cell were preserved through the process as each amplicon was tagged with a unique cell barcode. Pooled single cell DNA libraries were sequenced on Illumina MiSeq with paired-end multiplex runs (2 x 150 bp). Raw sequencing reads in FASTQ files were processed using the Tapestri Pipeline, which uses Bluebee's High Performance Genomics Platform. The pipeline trims adapter information, aligns sequences to the reference genome (hg19), assigns sequence reads to individual cell barcodes, calls genotypes using GATK, and generates annotated loom files which can be further analyzed in Tapestri Insights and H5 files which can be further analyzed in R. The number of cells sequenced per patient and the number of sequencing reads per cell are provided in **Table 4** of the **Supplementary Appendix.** Only mutations identified by both MSK-IMPACT (which excludes germline mutations using patient-specific control samples aforementioned) and single-cell DNA sequencing were used to construct the clonal architecture. Target loci included in **Fig. 1C-D** and **Fig. 2** in the **Supplementary Appendix** were genotyped in the majority of cells (median, 81%; IQR, 73-89%). Subclones from each sample were identified following exclusion of wild-type cells and cells with missing genotypes. Oncoprints were generated where each column represents an

individual cell and each row represents a mutation. Cells were clustered by subclone and then arranged by size of subclones from large to small. Subclones with <2% of mutant cells were removed, since such small subclones can represent false positive or negative genotypes as a result of allele-dropout or multiplets. The order of mutations in each sample was inferred based on the principle of maximum parsimony and depicted on fishplots in accordance with the proportions of the subclones. Small subclones that may result from allele-dropout were excluded from the fishplots.

DNA constructs and cell culture

BTK and *PLCγ2* cDNAs were subcloned into a lentiviral expression construct (Lenti-Ef1a-Puromycin-ZsGreen) and verified by Sanger sequencing. TMD8 and OCI-LY10 cells (provided as a gift from the Jonathan Schatz and Hans-Guido Wendel laboratories) were maintained in RPMI 1640 (Life Technologies, Grand Island, NY) with 2 mM L-glutamine, 20% fetal bovine serum (FBS) and 100 U ml^{-1} penicillin and 100 μg/ml streptomycin antibiotics. HEK 293T cells were grown in DMEM (Corning Cellgro) with 10% FBS, 100 U ml^{-1} penicillin and 100 μg /ml streptomycin. All transfections were performed in HEK293T cells using Polyethylenimine (PEI) reagent at 4:2:3 ratios of DNA construct: pVSVG: pPax2 in OPTI-MEM solution. Viral supernatant was collected 48 and 72 hours post-transfection. Spin-infections were performed at room temperature at 640 x g for 90 minutes with polybrene reagent (5μg/mL) (Fisher Scientific). Stably transfected TMD8 cells with *BTK* cDNA constructs were selected and maintained with puromycin (2 μg/mL) in cell culture medium.

Immunoblot assays

Whole cell lysates were prepared with Pierce IP lysis buffer supplemented with protease and phosphatase inhibitors (Thermo Scientific, Waltham, MA). Protein concentration was determined using BCA Protein Assay kit (Thermo Scientific, Waltham, MA). Ten μg of total protein was separated by electrophoresis on a 4-12% bis-tris protein gel, transferred onto a PVDF membrane and probed with antibodies against phospho-BTK (Tyr223), phospho-AKT (Ser473), Erk (Thr202/Tyr204), phospho-NF-κB p65 (Ser536), phospho-PLCγ2 (Tyr1217), total BTK, PLCγ2, AKT, NF-κB p65 and ERK1/2 from Cell Signaling Technologies (Danvers, MA). β-actin HRP (Sigma Aldrich #A3854) was used at 1:10,000. Membranes were visualized by ECL detection reagent (ThermoFisher) following the manufacturer's protocol.

BTK-drug affinity measurements

Surface plasmon resonance analysis (Biacore T200) was used to determine the inhibitor binding constants for the BTK proteins. Biotinylated WT, C481S, and T474I BTK proteins were purchased from CarnaBioscience while N-terminal DYKDDDDK (FLAG)-tagged, biotinylated A428D, M437R, and L528W BTK proteins (residues 2-659[end]) were expressed using a baculovirus expression system. BTK proteins were individually immobilized at a flow rate of 10 μL per min onto a Series S Streptavidin sensor chip (Cytiva) in a running buffer that consisted of 10 mM HEPES pH 7.4, 0.15 M NaCl, 10 mM $MgCl_2$, 2 mM DTT and 2% DMSO at 4°C. The assay was performed using the Biacore's single-cycle kinetics program at 4°C. Individual injection association and dissociation times were 120 seconds each with a final dissociation event of 2200 seconds. The flow rate throughout the kinetic analysis was 100 μL per min. The SPR sensorgrams were analyzed using Biacore Evaluation Software (version 3.2.1).

Cell line RNA-seq and analyses

For cell line RNA sequencing (RNA-seq), RNA was extracted from TMD8 cells using the Qiagen RNeasy extraction kit, according to the manufacturer's instructions. A minimum of 500 ng of high-quality RNA (as determined by Agilent Bioanalyzer) per replicate was used as input for library preparation. Poly(A)-selected, strand-specific (dUTP method) Illumina libraries were prepared by the Integrated Genomics Operation (IGO) at Memorial Sloan Kettering with a modified TruSeq protocol and sequenced on the Illumina HiSeq 2000 to obtain ~50-60M 2x101 bp paired-end reads per sample. FASTQ files were first trimmed using Trim_galore (v0.6.4) to remove sequencing adapters and low quality (Q<15) reads. Trimmed sequencing reads were aligned to the human Hg19 reference genome (GENCODE, GRCh37.p13) using STAR (v2.7.5)[8]. SAM files were subsequently converted to BAM files, sorted, and indexed using samtools (v1.9). BAM files were used to generate bigwig files using bamCoverage (part of the Deeptools package; v3.3.1). Read counting across genomic features was performed using featureCounts (part of the subread package; v1.5.0)[9] with the following parameters: -p -T 20 -O -F GTF -t exon. Differential gene expression analysis (DGEA) was performed using the edgeR (v3.32.1) and Limma/Voom (v3.46.0) workflow[10]. DGEA lists were pre-ranked (by t-statistic) and used an input for gene set enrichment analyses (GSEA) using GSEA software (Broad Institute; https://www.gsea-msigdb.org/gsea/index.jsp) against the following signatures in the Molecular Signatures Database (MSigDB) collection: regulatory target gene sets (C3). Data visualization and figure generation was performed in Rstudio (v1.3.1073) using the following packages: ggplot2 (v3.3.5), ggpubr (v0.4.0), and complexHeatmap (v2.6.2).

Competition-based and cell viability assays

Competition assays were performed using OCI-LY10 cells transduced with *BTK* or *PLCγ2* cDNA constructs and mixed with parental cells at fixed ratios, followed by 4 days of treatment with either vehicle (DMSO) or the BTK inhibitors pirtobrutinib (LOXO Oncology), ibrutinib (SelleckChem), fenebrutinib (SelleckChem), ARQ-531 (SelleckChem), and vecabrutinib (MedChem Express). GFP percentages were analyzed using BD LSR Fortessa Flow Cytometer. GFP percentages were plotted as a heatmap depicting GFP fold change normalized to vehicle (DMSO). Cell viability assays were performed with TMD8 cells stably expressing *BTK* constructs. These cells were plated (25,000 cells/well in triplicates per concentration) in opaque-walled 96-well plates and treated for 3 days with varying concentrations (10 pM to 100 μM) of pirtobrutinib, ibrutinib or fenebrutinib. Cell viability was measured with CellTiter-Glo Luminescent reagent (Promega) according to the manufacturer's instructions. Absolute viability values were converted to percentage viability normalized to DMSO control. Non-linear fit of log (inhibitor) versus response was calculated in GraphPad Prism v9.0 to obtain IC_{50} values.

Ca^{+2} mobilization and IP1 release assay

Intracellular calcium levels in TMD8 cells expressing BTK WT, V416L, A428D, M437R or L528W were measured using Indo-1 (Life Technologies) on an LSR-Fortessa-HTS flow cytometer. Indo-1 Violet and Indo-1 Blue levels were measured for two minutes immediately followed by stimulation with 10μg/mL of anti-human IgM (Southern Biotech) and then measured continuously for 10 minutes. Inositol monophosphate (IP1), a stable downstream metabolite of inositol triphosphate (IP3) induced by activation of a phospholipase C (PLC) cascade was measured using IP1 Elisa kit (Cisbio). TMD8 cells expressing BTK WT, V416L, A428D, M437R or L528W, were stimulated with 10μg/mL of anti-human IgM (Southern Biotech) for 15 minutes and lysed; IP1 was stabilized with LiCl and conjugated using IP-1 HRP and IP-1 mAb. Absorbance was measured at 450nm using a Synergy 2 Biotech plate reader.

Structural modeling

Molecular graphics and analyses were performed with UCSF ChimeraX[11]. The published structures of ibrutinib (PDB 5P9J[12]) and ARQ-531 bound to BTK (PBD 6E4F[13]) were used to map patient mutations onto the BTK kinase domain. Pirtobrutinib was modeled into BTK structure using induced fit docking and binding pose metadynamics[14] in the Schrödinger Suite (ver. 2021-1, Schrödinger Inc., NY, NY) with ibrutinib-bound BTK as a model. ATP was modeled into the BTK active site in Schrödinger using the structure of SRC kinase bound to an ATP analogue (PDB 3DQW[15]) as a guide.

CITE-seq experimental workflow

Healthy donor PBMCs were obtained from StemCell Technologies from donors between the ages of 46-58 years old. Frozen PBMCs from CLL patients were briefly thawed and transferred into 50 ml conical tubes. 25 mls of pre-warmed RPMI 1640 (Corning) supplemented with 20% FBS was added dropwise to tubes. Cell suspensions were subjected to centrifugation at 400 x g for 5 minutes and supernatant was discarded. Pellets were resuspended in 1X PBS with 2% FBS and filtered using a 70 μm nylon mesh (ThermoFisher). Subsequently, cells were stained with TruStain FcBlock (BioLegend) at 1:100 and incubated on ice for 5 minutes. Individual samples (healthy; pre- and post-pirtobrutinib PBMCs) were then incubated with unique barcoded TotalSeq-A Cell Hashing reagents (1:100) for 15 minutes on ice and subsequently stained with FITC-conjugated CD19, APC-conjugated CD5, and PerCP-conjugated CD45 for 30 minutes on ice. Following incubation, cell suspensions were subjected to three wash cycles involving resuspension of cell pellets in 3ml PBS with 2% FBS, followed by centrifuging at 400 x g at 4 degrees Celsius for 5 minutes. Finally, samples were resuspended in 500 μls of PBS with 2% FBS and supplemented with 4',6-diamidino-2-phenylindole (DAPI) (0.5 μg/ml) for live/dead staining. Cell sorting was performed using SY3200™ highly automated parallel sorting (HAPS) cell sorter. All samples were gated based on forward and side scatter, followed by exclusion of doublets, then gated on viable $DAPI^{low}$ cells. For healthy donors, PBMCs were sorted on $CD45^+$ cells into 1.5 ml tubes containing 200 μl ice-cold RPMI 1640 with 10% FBS. PBMCs from CLL patients were sorted into two fractions: $CD19^+$ (CLL/B-cells) or $CD45^+CD19^-$ (non-CD19 immune cells) into individual 1.5 ml tubes containing 200 μl ice-cold RPMI 1640 with 10% FBS. After cell sorting, CLL sorted fractions, $CD19^+$ (CLL/B-cells) and $CD45^+CD19^-$ (non-CD19 immune cells) were manually mixed at approximately a 1:4 ratio ($CD19^+$: $CD45^+CD19^-$) for each sample. Cells were then spun down at 400 x g at 4°C for 5 minutes and incubated with TotalSeq™ -A Human Universal Cocktail (BioLegend) according to manufacturer's instructions. The libraries were prepared using the Chromium Single Cell 3′ Reagent Kits (v2 and v3): Single Cell 3′ Library & Gel Bead Kit v2 (PN-120237), Single Cell 3′ Library & Gel Bead Kit v3 (PN-1000075), Single Cell 3′ Chip Kit v2 (PN-120236), Chromium Next GEM Chip G Single Cell Kit (PN-100120) and i7 Multiplex Kit (PN-120262) (10x Genomics)[16] and following Single Cell 3′ Reagent Kits (v2) User Guide (manual part no. CG00052 Rev A) and Single Cell 3′ Reagent Kits (v3) (manual part no. CG000183 Rev C). Libraries were pooled consisting of 70% cDNA, 25% antibody-derived tags (ADTs), and 5% protein-tag and sequenced on an Illumina NOVA-seq S2 paired-end reads, at one full lane per sample (26 cycles read 1, 8 cycles index, and 91 cycles read 2).

CITE-seq data analysis

Raw sequencing reads in FASTQ files were processed in a cloud-based environment using Cumulus workflows.[17] The Cell Ranger pipeline extracts cell barcodes, unique molecular identifiers (UMI), cDNA reads, and antibody barcodes; aligns cDNA reads to the human GRCh38 reference genome; and generates gene and antibody UMI count matrices. The Demultiplexing pipeline uses cell hashing to assign cell barcodes to specific patient samples and droplet types (singlet, doublet, or unknown).[18] Cells that passed the following QC filters were included in downstream analysis: 1) singlets identified by cell hashing, 2) cells with >500 and <7000 detected genes (outliers may represent empty droplets, low quality cells, doublets, or multiplets), 3) cells with <50,000 cDNA UMI and <10,000 ADT UMI (outliers may represent doublets or multiplets or cells with aberrant clumps of antibodies), and 4) cells with <0% mitochondrial gene expression (extensive mitochondrial contamination often characterizes low quality or dying cells) (**Figure 5B** in the **Supplementary Appendix**). 53,722 cells across 17 samples passed QC and were included in downstream analysis (**Figure 5C** in the **Supplementary Appendix**).

Each CITE-seq sample was mapped to a previously described CITE-seq reference atlas of 162,000 PBMC measured with 228 antibodies.[19] Briefly, each dataset was normalized using regularized negative binomial regression for the RNA assay and centered-log ratio for the ADT assay, anchors were identified between samples and reference using a pre-computed supervised PCA transformation, and then samples were projected onto the UMAP structure of the reference with transfer of the cell type labels from the reference. Annotated cell types were confirmed by considering each cluster's differentially expressed genes together with known cell type markers including CD19, CD200, CD4, CD8, CD56, CD16, CD14, and CD11c (**Figure 5C** in the **Supplementary Appendix**).

B/CLL cells were integrated across patient samples using LIGER (linked inference of genomic experimental relationship), an algorithm that employs integrative non-negative matrix factorization (iNMF) to identify shared cell states or gene expression programs across heterogeneous single-cell datasets.[20] Briefly, samples were subset by PBMC cell types identified by reference mapping as described above and then preprocessed to produce raw digital gene expression matrices, followed by normalization of expression data to account for differences in sequencing depth and efficiency between cells, identification of highly variable genes (n = 2,000), and scaling of individual genes without centering as iNMF requires non-negative values. Next, iNMF was performed on normalized and scaled data to identify shared

factors or gene expression programs across patient samples. Joint clustering of cells was performed using maximum factor loading in each cell followed by construction of a shared factor neighborhood graph, in which cells with similar factor loading or gene expression programs were connected. An arbitrary number of factors was chosen after testing a range of factors and ensuring the overall conclusions were robust.

Statistical Analysis

Differential gene expression analysis (DGEA) on bulk RNA-seq was performed using the edgeR (v3.32.1) and Limma/Voom (v3.46.0) analysis software. DGEA lists were pre-ranked (by t-statistic) and used an input for gene set enrichment analyses (GSEA) using GSEA software (Broad Institute). Statistical comparisons of module scores across single-cell RNA-seq conditions were performed using a two-sided Wilcoxon Rank Sum test. Comparisons of IP1 formation were performed by analysis of variance (ANOVA) with Tukey's multiple-comparison correction.

Statistical analysis used for comparing single-cell RNA expression of B-cell receptor signaling pathway: the B-cell receptor (BCR) signaling pathway gene set consists of 75 genes and was obtained from the Molecular Signatures Database (MSigDB). Expression of the gene set was scored using *AddModuleScore*, which calculates the average expression levels of all the genes in a given gene set and then subtracts the average expression levels of control gene sets.[15] All genes were binned based on their average expression, and 5 control genes were randomly selected from each bin. This method controls expression of the gene set for differences in cell quality and library complexity across single cells. Statistical comparisons of the BCR signaling pathway module scores between matched pre- and post-treatment samples and across treatment conditions were performed using a two-sided Wilcoxon Rank Sum test.

Additional Study Patient Details and Histories

Patient ID1

46-year-old male diagnosed with CLL approximately 8 years prior to initiation of pirtobrutinib. He was treated with multiple therapies including chemoimmunotherapy (fludarabine, cyclophosphamide, rituximab followed by bendamustine and rituximab) and then ibrutinib for 26 months. Following ibrutinib discontinuation for progression of CLL he received multiple additional treatments including idelalisib, mini-R-CHOP (rituximab, cyclophosphamide, doxorubicin, vincristine, prednisone), venetoclax as monotherapy, and then in combination with ibrutinib, high-dose methylprednisone combined with obinutuzumab, 1929z-1BBL chimeric

antigen receptor (CAR) T-cell therapy, focal radiotherapy to the mandible, and then umbralisib, ublituximab, and pembrolizumab on a clinical trial. Given progressive CLL, he was started on pirtobrutinib monotherapy which he continued for 11 months with a best response of partial response with lymphocytosis (PR-L). He had progressive CLL with increasing lymph nodes and splenomegaly leading to discontinuation of pirtobrutinib. He has been subsequently treated.

Patient ID2

60-year-old female diagnosed with CLL approximately 7 years prior to initiation of pirtobrutinib. Within a month of her diagnosis, she received bendamustine and rituximab (BR, four cycles). Two years later, in relapse she was treated with an additional 4 cycles of BR with partial response. Within 4 months of BR she relapsed and received ibrutinib for 23 months prior to discontinuing for disease progression. She was then treated with venetoclax for nine months prior to discontinuation for disease progression. She was then treated with SNS-062 (vecabrutinib) for approximately 1 month with no response. Subsequently, she received an anti-CD20 x anti-CD4 bispecific monoclonal antibody on a clinical trial with no response. She was then treated with multiple chemotherapy-based regimens including Hyper-CVAD (cyclophosphamide, vincristine, doxorubicin, dexamethasone), EPOCH (etoposide, prednisone, vincristine, cyclophosphamide, doxorubicin), and then ofatumumab and venetoclax with disease progression after 1 cycle of each regimen. She received ninth-line therapy with duvelisib for 3 months and then had progressive CLL. Following all of this, she was treated with pirtobrutinib as tenth-line therapy for her CLL for 6 months with a best response of stable disease and discontinued for disease progression manifesting as increasing lymph node sizes and splenomegaly. She was managed supportively and died shortly after discontinuing treatment.

Patient ID3

Patient 3 was a 53-year-old female diagnosed with CLL approximately 9 years prior to pirtobrutinib initiation. She was managed with observation for 21 months prior to treatment with R-CVP (rituximab, cyclophosphamide, vincristine, prednisone) with 4 cycles of therapy. She was observed for 18 months and then started second line treatment with fixed duration venetoclax in combination with rituximab for 25 months. Fourteen months later she was started on ibrutinib which she continued for approximately 19 months prior to discontinuation for progressive CLL. She was started on fourth-line treatment with pirtobrutinib with best response of stable disease. She remained on pirtobrutinib for 9 months but developed CLL disease progression with a rising absolute lymphocyte count on treatment. Following pirtobrutinib discontinuation, she received additional treatment.

Patient ID4

54-year-old female diagnosed with CLL approximately 19 years prior to pirtobrutinib initiation. She was observed for approximately 2 years and treated with RFM (rituximab, fludarabine and mitoxantrone). Approximately 4.5 years later, she had progressive CLL that was treated with R-CVP chemoimmunotherapy with one cycle of rituximab maintenance. Approximately 46 months later, she was treated with BR resulting in a 34-month remission prior to disease progression. She was next treated with ibrutinib for 57 months prior to developing disease progression. Following this, she was treated with pirtobrutinib with a best response of stable disease. After 11 months of pirtobrutinib she experienced disease progression with increasing lymph nodes and rising absolute lymphocyte count and received subsequent treatment for her CLL.

Patient ID5

56-year-old female diagnosed with CLL approximately 12 years prior to pirtobrutinib initiation. She was observed for 32 months prior to initiation of fludarabine, rituximab and cyclophosphamide (FCR). Approximately 33 months following therapy completion she had disease progression and was treated with bendamustine and rituximab/ofatumumab. After 23 months of remission she was treated with ibrutinib for 42 months. She then initiated pirtobrutinib with a best response of partial response and developed CLL progression with increasing lymph nodes and a rising absolute lymphocyte count after 17 months of treatment. She received subsequent treatment.

Patient ID6

39-year-old male diagnosed with CLL approximately 10 years prior to pirtobrutinib initiation. He was observed for 6 years prior to initiation of chemoimmunotherapy with FCR. Thirty months following the completion of FCR he had progressive CLL and was treated with ibrutinib for 9 months prior to discontinuing for disease progression. He then was treated with umbralisib, ublituximab, and pembrolizumab on a clinical trial for 2 months but experienced CLL progression. He initiated fourth-line treatment with pirtobrutinib with a best response of stable disease. Pirtobrutinib was discontinued after 3 months of treatment due to progressive CLL with increasing lymph nodes. He subsequently received additional treatment.

Patient ID7

55-year-old male diagnosed with CLL approximately 1 year prior to pirtobrutinib initiation. He was treated with 2 cycles of FCR with primary refractory disease and then started on ibrutinib

for 10 months prior to developing disease progression. He was treated with pirtobrutinib as third-line therapy with a best response of stable disease. He developed increasing lymphadenopathy with biopsy demonstrating Richter transformation (RT) to diffuse large B-cell lymphoma (DLBCL) leading to discontinuation of pirtobrutinib after 5 months of treatment. He subsequently received treatment for RT.

Patient ID8

51-year-old male diagnosed with CLL approximately 18 years prior to pirtobrutinib initiation. Approximately two years following CLL diagnosis he was treated with weekly rituximab followed by monthly rituximab. He was then treated with fludarabine and cyclophosphamide for 6 cycles. Nine months after finishing treatment he initiated third line lenalidomide with dexamethasone. Rituximab was then added to lenalidomide approximately three years later. In total he received approximately 46 months of lenalidomide-based therapy. He was then treated with ibrutinib for 89 months. This was discontinued due to disease progression. He was treated subsequently with venetoclax and obinutuzumab was added to venetoclax after 14 months for a total of 20 months of venetoclax-based therapy. He was started on pirtobrutinib with a best response of partial response. He had disease progression with increasing lymph nodes and rising absolute lymphocyte count and bone marrow biopsy showed Richter transformation to DLBCL. He discontinued pirtobrutinib after 9 months of treatment. He received subsequent treatment.

Patient ID9

48-year-old male diagnosed with CLL approximately 10 years prior to treatment with pirtobrutinib. After a two-year period of initial observation, he was treated with FCR for 5 cycles followed by two years of maintenance rituximab. Twenty-two months following completion of rituximab he had progressive disease and was treated with six cycles of BR. He had a remission of 15 months prior to treatment with ibrutinib which he continued for 56 months prior to discontinuing for rash and disease progression. He was then treated with venetoclax in combination with rituximab and then venetoclax in combination with ibrutinib for a total of 7 months of venetoclax-based therapy prior to discontinuation for CLL progression. He was treated with pirtobrutinib with a best response of partial response. After 13 months of pirtobrutinib he developed disease progression with increasing lymph nodes leading to discontinuation of pirtobrutinib. Bone marrow biopsy showed Richter transformation to DLBCL. He received additional treatment.

Figure S1

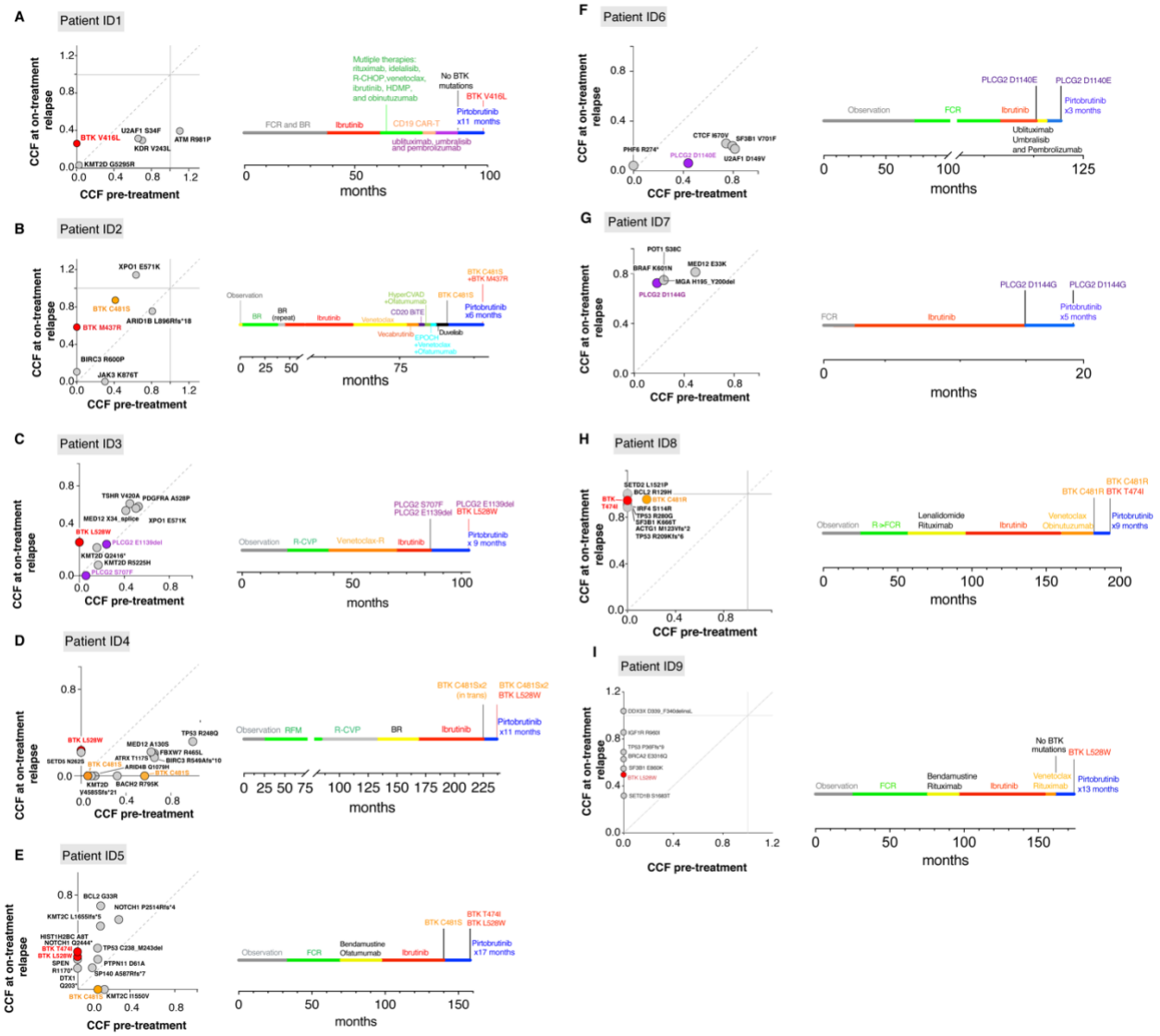

Figure S1. BTK and PLCγ2 mutations seen in patients with resistance to non-covalent BTK inhibition. All patient treatment courses with time on prior therapies and the non-covalent BTK inhibitor pirtobrutinib shown in months (**Panels A-I**). BR = bendamustine, rituximab; EPOCH = etoposide, prednisone, vincristine, cyclophosphamide, doxorubicin; FCR = fludarabine, cyclophosphamide, rituximab; HyperCVAD = hyperfractionated cyclophosphamide, vincristine, doxorubicin, dexamethasone; R-CVP = rituximab, cyclophosphamide, vincristine, prednisone; RFM = rituximab, fludarabine, mitoxantrone; Ven-R = venetoclax, rituximab; HDMP = high dose methylprenisone; BiTE = bi-specific T-cell engager antibody. For time-limited therapies, bar represents both the treatment course and period of observation prior to next line of therapy.

Figure S2

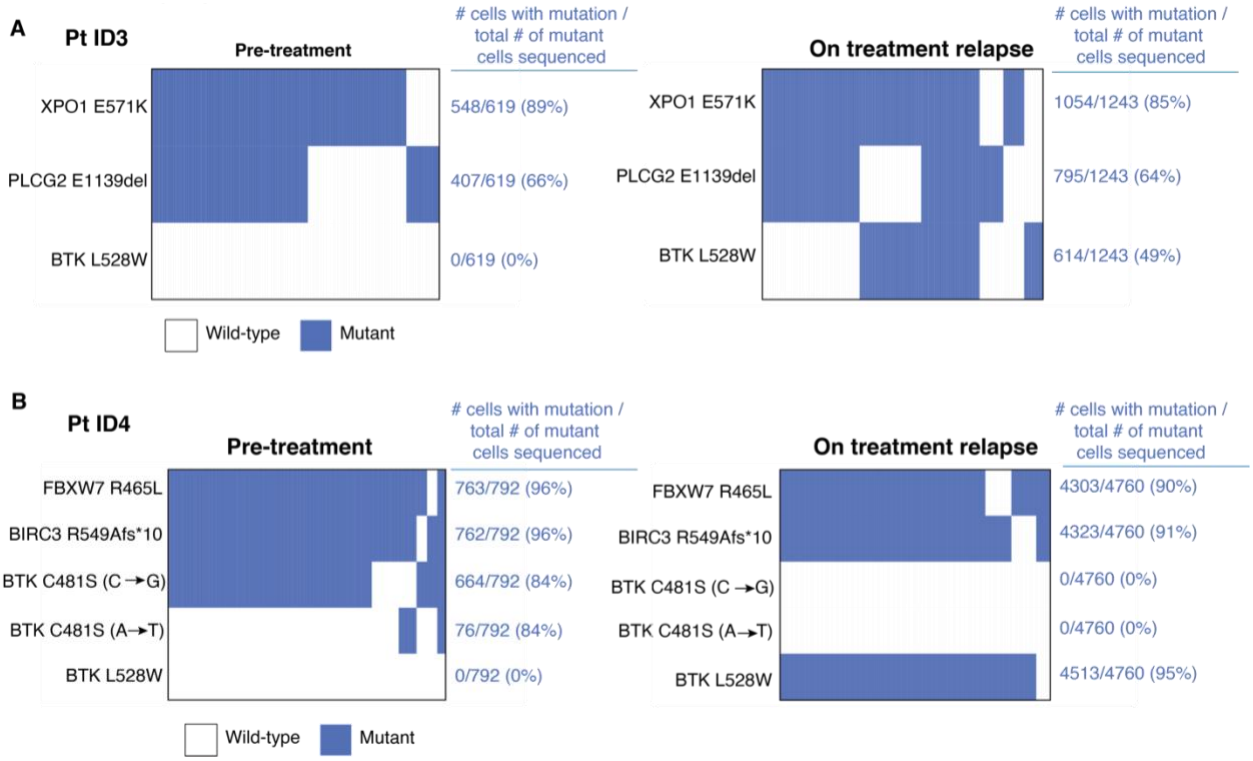

Figure S2. Single cell mutational analyses of patients developing on-treatment relapse to pirtobrutinib. Oncoprints of mutations in single cells sequenced from Patient ID3 (**Panel A**) and ID4 (**Panel B**) prior to pirtobrutinib (left) and at the time of on-treatment relapse. Each column (vertical line) in the oncoprint represents an individual cell and each row indicates the genotype for each variant. Cells were clustered by subclone and then arranged by size of subclones from large to small. Mutant and wild-type cells are indicated in blue and white, respectively. The number of cells with each mutation, total number of mutant cells, and percentage of mutant cells with each mutation is indicated on the right of each oncoprint. For Patient ID3, the BTK L528W mutation was not present pre-treatment but was detected in 614 out of 1,243 cells sequenced at the time of on-treatment relapse, 258 of which contained co-existing PLCG2 mutations. Patient ID4 had two distinct BTK C481S mutations (generated by two distinct nucleotide substitutions as indicated in the figure) prior to treatment with pirtobrutinib. On treatment relapse, the BTK C481S mutations were no longer present and instead BTK L528W mutations were detected in 4,513 cells, representing 95% of mutant cells.

Figure S3

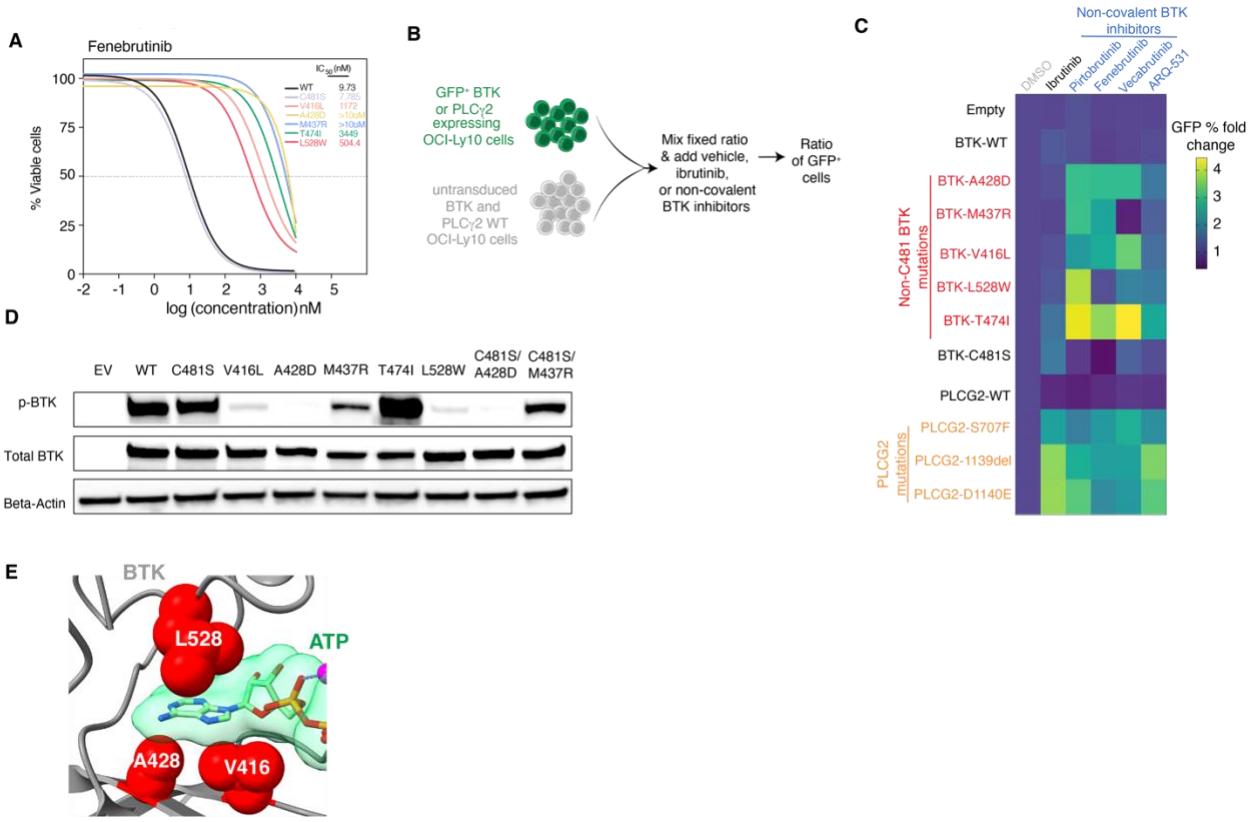

Figure S3. Characterization of BTK mutations conferring resistance to non-covalent BTK inhibitors. IC_{50} curves for the noncovalent BTK inhibitor fenebrutinib are shown in **Panel A**. Competition-based assay in OCI-Ly10 human BTK-dependent human B-cell lymphoma cells upon lentiviral transduction of wild-type (WT) or mutant BTK or *PLCγ2* constructs expressing GFP (**Panel B**). Lentiviral transduction of OCI-Ly10 cells with BTK and PLCγ2-mutant cDNA constructs were mixed with untransduced OCI-Ly10 cells at fixed GFP ratios and subsequently treated with indicated BTK inhibitors for four days. GFP percentages were then measured using flow cytometry. Cells treated with non-covalent BTK inhibitors for four days showed positive selection of PLCγ2 (S707F, E1139del, and D1140E) mutations (**Panel C**). Transduction of HEK293T cells with lentiviral BTK cDNA constructs shows BTK-V416L, -A428D, -L528W, and -C481S/A428D lack BTK phosphorylation at Y223 (**Panel D**). Model of ATP (green) bound by the BTK kinase domain (gray) based on the structure of SRC kinase bound to an ATP analogue (PDB 3DQW). BTK residues mutated in pirtobrutinib resistant patients are shown as red spheres. A428, V416, and L528 interact with ATP in this model, and their mutation abrogates kinase activity (**Panel E**).

Figure S4

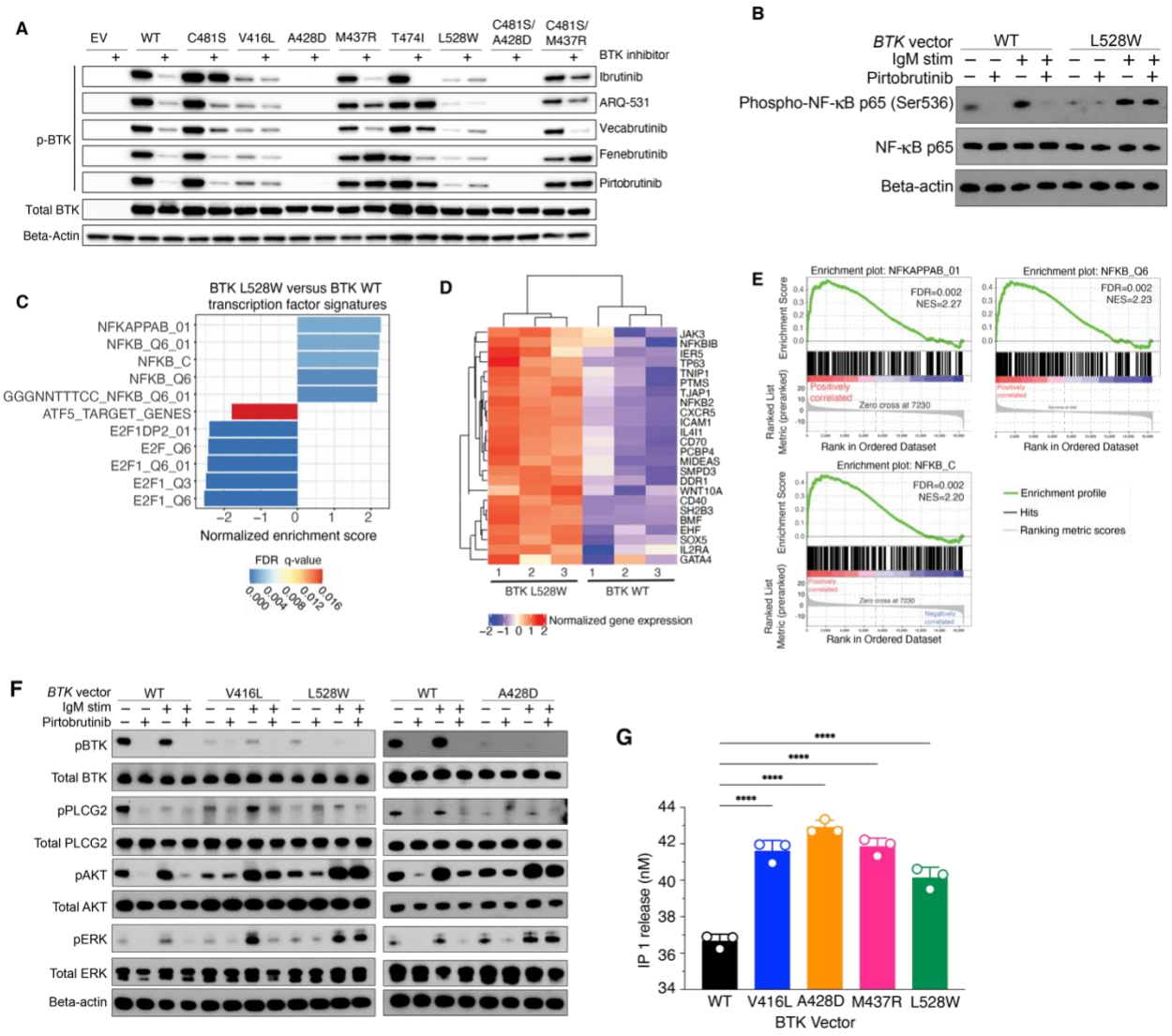

Figure S4. Effect of non-C481 BTK mutations on B-cell receptor signaling and response to BTK inhibitors. Transduction of HEK293T cells with BTK cDNA constructs exposed to the non-covalent BTK inhibitors (ARQ-531, vecabrutinib, fenebrutinib, and pirtobrutinib) and covalent BTK inhibitor, ibrutinib (**Panel A;** "+" sign indicates presence of drug). In the presence of IgM stimulation, TMD8 cells transduced with L528W mutant BTK have enhanced activation of NF-kB (as indicated by enhanced phosphorylated p65 (phosphorylated Serine 536 (Ser536)) and sustained p-p65 despite treatment with pirtobrutinib. (**Panel B**) Enrichment of top-ranked regulatory target gene sets (C3; MSigDB) from Gene Set Enrichment Analysis (GSEA) comparing RNA-seq data from BTK^{WT} to BTK^{L528W} TMD8 cells (**Panel C**). Row-scaled heatmap of normalized (counts per million) gene expression values from BTK^{WT} and BTK^{L528W} samples for genes common to NFKAPPAB_01, NFKB_Q6_01, and NFKB_C gene sets (*from C*) (**Panel D**). GSEA enrichment plots for NFKAPPAB_01, NFKB_Q6_01, and NFKB_C gene sets (*from C*) comparing BTK^{WT} to BTK^{L528W} (**Panel E**). In the presence of IgM stimulation, TMD8 cells transduced with catalytic-inactive BTK mutations treated with pirtobrutinib sustain activation of AKT (phosphorylated S473) (**Panel F**). Bar graphs of IP1 (inositol monophosphate) release from

BTK WT or mutant TMD8 cells following IgM stimulation (**Panel G**). ****p<0.001 by analysis of variance (ANOVA), with Tukey's multiple-comparisons correction.

Figure S5

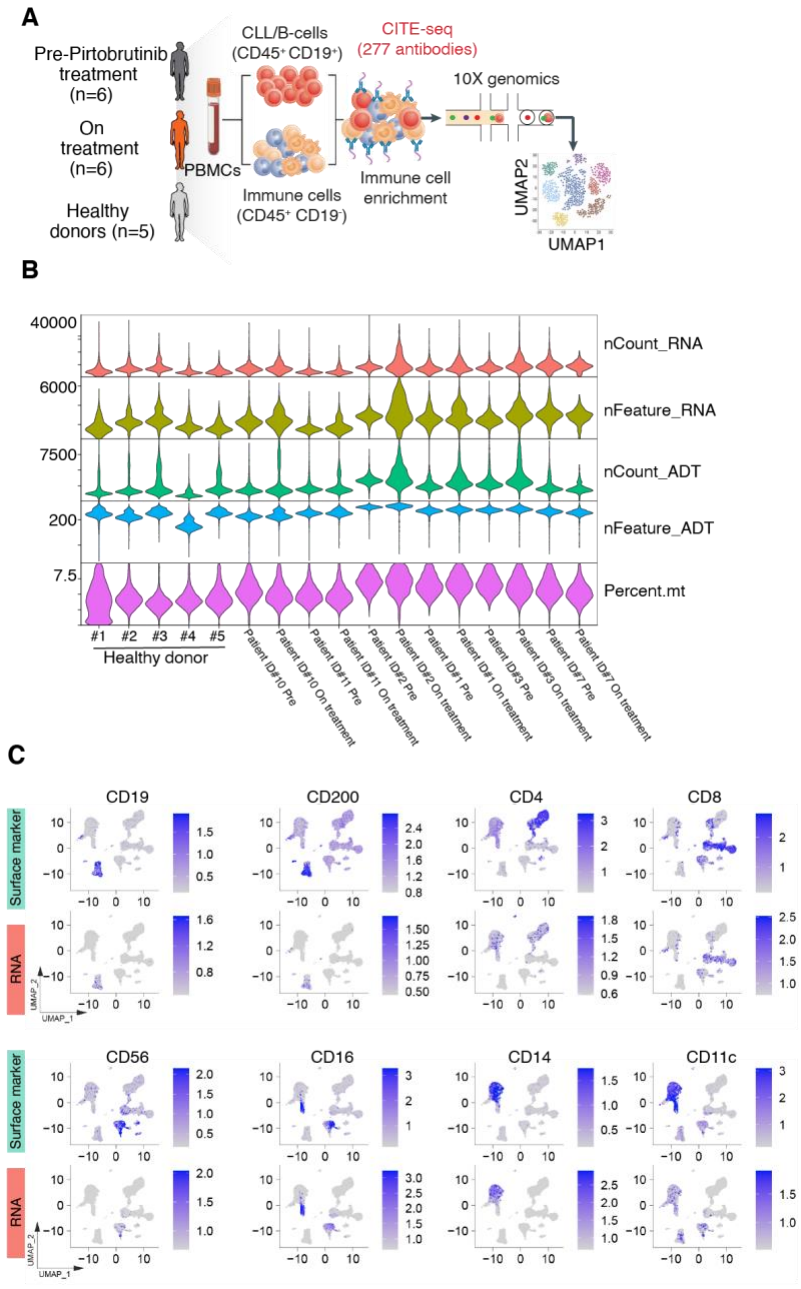

Figure S5. Method and quality assessment of multimodal single-cell analysis of pirtobrutinib patients. Schematic of Cellular Indexing of Transcriptomes and Epitopes by sequencing (CITE-seq) of six paired peripheral blood mononuclear cell (PBMC) patient samples pre-treatment and on treatment with pirtobrutinib as well as five approximately age-matched healthy donor PBMCs (**Panel A**). Flow cytometry sorting of PBMCs from CLL patients into B/CLL ($CD19^+CD45^+$) and immune cell ($CD19^-CD45^+$) fractions was performed to enrich for immune cell types. Violin plots showing quality metrics of single cells included in downstream analysis (**Panel B**). nCount RNA: number of RNA unique molecular identifiers (UMI); nFeature RNA: number of detected genes; nCount_ADT: number of antibody UMI; nFeature_ADT:

number of detected antibodies; percent.mt: percentage of mitochondrial gene expression. Cells with <500 and >7000 detected genes were removed as they often represent empty droplets, low quality cells, doublets, or multiplets. Cells with >50,000 RNA UMI and >10,000 ADT UMI were also removed as they often represent doublets, multiplets, or cells with aberrant clumps of antibodies. Cells with >10% mitochondrial gene expression were excluded as low quality or dying cells often demonstrate extensive mitochondrial contamination. UMAP projection of surface proteins (top) and corresponding mRNA (bottom) used to confirm the six broad hematopoietic cell types identified by multimodal PBMC reference mapping, (**Panel C**). B-cell/CLL cluster (CD19 and CD200), $CD4^+$ T-cell cluster (CD4), $CD8^+$ T-cell cluster (CD8), monocyte cluster (CD14, CD16, and CD11c), and NK-cell cluster (CD56, CD16).

Figure S6

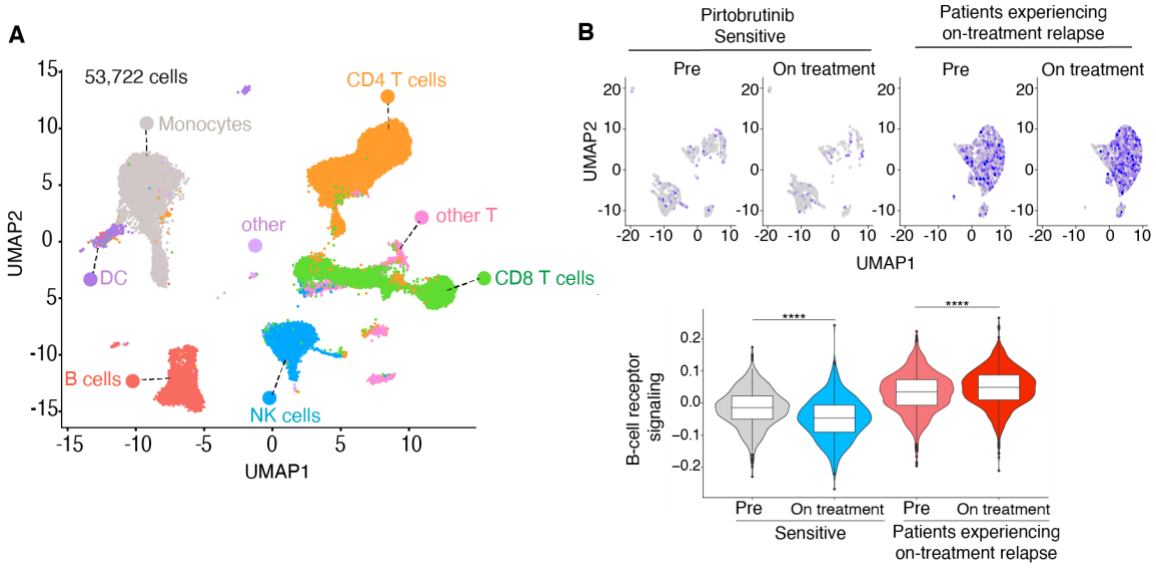

Figure S6. Persistent transcriptional activation of B-cell receptor signaling within individual CLL cells from patients with on-treatment relapse to pirtobrutinib.
53,722 cells from 17 samples were mapped to a previously described multimodal PBMC reference atlas[18], and six broad immune cell types were annotated (monocytes, dendritic cells, $CD4^+$ T, $CD8^+$ T, B, and natural killer (NK) cells) (**Panel A**). Each cell type was integrated across patient samples and jointly analyzed using LIGER (linked inference of genomic experimental relationship). Average expression of B-cell receptor (BCR) pathway genes (n = 75) in the B/CLL subset (**Panel B**). Patients with ongoing response to pirtobrutinib (n=2) showed decreased BCR pathway expression (p-value < 0.001, Wilcoxon Rank Sum test), while patients with on-treatment relapse (n=4) showed increased expression (p-value < 0.001). Even at baseline, pre-treatment CLL cells from patients who developed resistance have higher expression of the BCR pathway than pre-treatment CLL cells from patients with ongoing response to pirtobrutinib (p-value < 0.001).

Figure S7

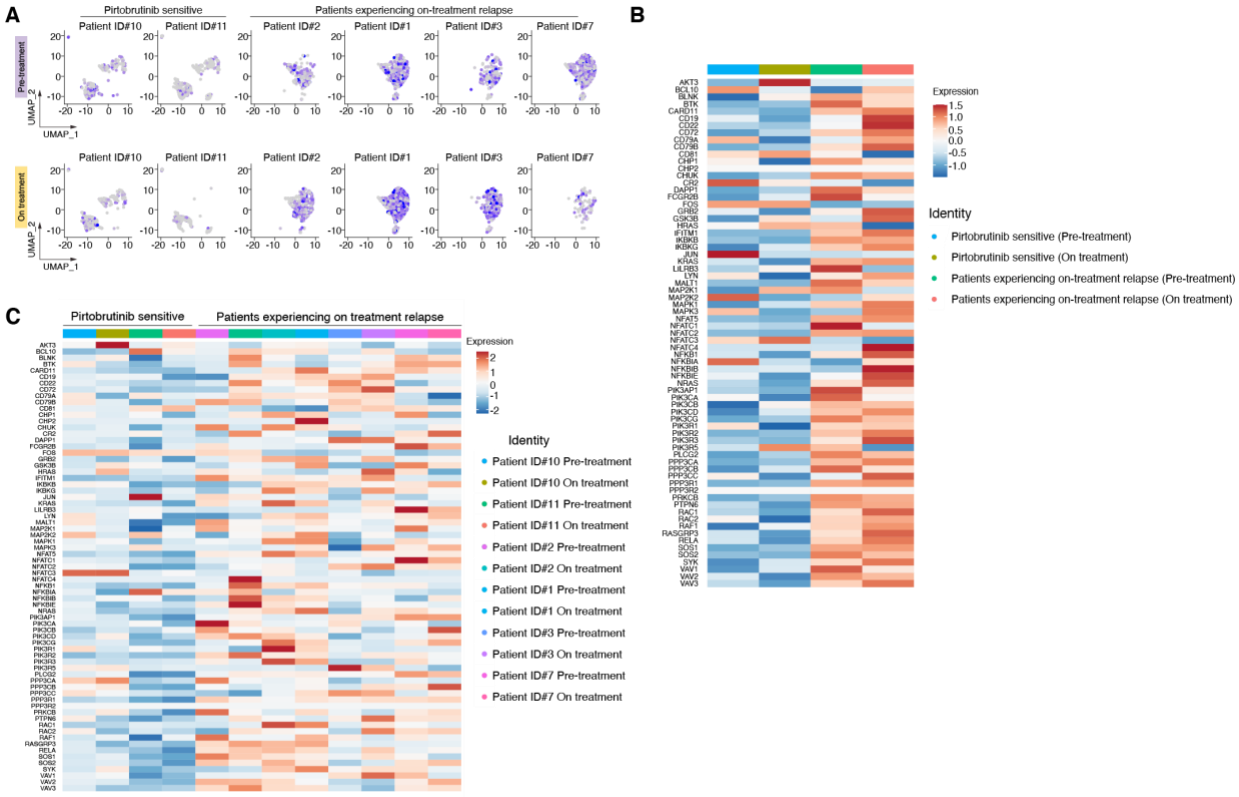

Figure S7. Increased transcriptional activation of B-cell receptor signaling in patients with acquired resistance to pirtobrutinib versus patients with ongoing response. Average expression of B-cell receptor pathway genes (n = 75) in the B/CLL subset of peripheral blood mononuclear cells collected pre-treatment and on-treatment from 2 patients with ongoing response to pirtobrutinib and 4 patients with on-treatment relapse (**Panel A**). Heatmap of the B-cell receptor pathway gene set in pre- and on-treatment samples from patients who remain sensitive vs. patients who acquired resistance to pirtobrutinib (**Panel B**). Per sample view of the heatmap in Panel B (**Panel C**).

Table S1. Characteristics of CLL patients with acquired resistance to pirtobrutinib.

ID	Age (yrs)[#]	Sex	Prior Therapy (no.)	Prior Covalent BTKi	Pre-pirtobrutinib BTK/PLCγ2 Mutations (CCF; Site Tested)	Best Clinical Response *	Time on Pirtobrutinib Therapy (mos.)	Key Mutations at Disease Progression on Pirtobrutinib (CCF; Site Tested)##	Clinical Characteristics of CLL Progression	Used in single cell mutational analyses (Fig. 1)	Used in CITE-seq analyses (Fig. 4)
1	54	M	10	ibrutinib	No	PR-L	11	BTK V416L (0132; Site: BM; LN)	Increasing lymph nodes and spleen.	-	Yes
2	67	F	9	ibrutinib	BTK C481S (0.412) (PB)	SD	6	BTK M437R (0.584; Site: LN)	Increasing lymph nodes and spleen.	-	Yes
3	62	F	3	ibrutinib	PLCγ2 S707F (0.24) PLCγ2 E1139del (0.058)(BM)	SD	9	BTK L528W PLCγ2 E1139del (0.298; 0.280; Site: PB; BM)	Rising absolute lymphocyte count.	Yes	Yes
4	73	F	4	ibrutinib	BTK C481S x 2 (0.060 and 0.566) (BM)	SD	11	BTK L528W (0.578; Site: BM)	Increasing lymph nodes. Rising absolute lymphocyte count.	Yes	-
5	68	F	3	ibrutinib	BTK C481S (0.184) (PB)	PR	17	BTK T474I BTK L528W (0.334; 0.288; Site: BM)	Increasing lymph nodes. Rising absolute lymphocyte count.	-	-
6	48	M	3	ibrutinib	PLCγ2 D1140E (0.440) (LN)	PR	3	PLCγ2 D1140E (0.062; Site: LN)	Increasing lymph nodes.	-	-
7**	56	M	2	ibrutinib	PLCγ2 D1144G (0.186) (PB)	SD	5	PLCγ2 D1144G (0.724; Site: LN)	Increasing lymph nodes with lymph node biopsy confirming RT DLBCL.	-	Yes
8**	69	M	5	ibrutinib	BTK C481R (0.160) (PB)	PR	9	BTK T474I (0.944; Site: PB; LN)	Increasing lymph nodes. Bone marrow biopsy showing RT DLBCL. Rising absolute lymphocyte count.	-	-
9**	62	M	4	ibrutinib	No (BM)	PR	13	BTK L528W (0.256; Site: BM; LN)	Increasing lymph nodes. Bone marrow biopsy confirming RT DLBCL.	-	-

Abbreviations: BM = bone marrow, BTK = Bruton's tyrosine kinase, BTKi = Bruton's tyrosine kinase inhibitor, CCF= cancer cell fraction; CLL= chronic lymphocytic leukemia, DLBCL= diffuse large B-cell lymphoma, F = female, LN = lymph node, M = male, mos = months, PB = peripheral blood, PLCγ2 = phospholipase C gamma 2, PR = partial response, PR-L = partial response with lymphocytosis, yrs = years, no. = number, SD = stable disease, RT = Richter Transformation.

[#]Age is designated at the time of pirtobrutinib therapy initiation.

All samples were either collected on-treatment or +/- 23 days from the time of drug discontinuation except for patient 8 who had new mutation first detected at the time of early progression 52 days prior to discontinuation of pirtobrutinib and then again 31 days prior to drug discontinuation.

*Responses were assessed according to the International Workshop on Chronic Lymphocytic Leukemia (IwCLL) 2018 guidelines.

**Patients 7, 8, and 9 had progression of disease with Richter transformation to DLBCL.

Table S2. Pre-pirtobrutinib molecular features of CLL patients who acquired resistance to pirtobrutinib.

ID	IGHV Mutation Status	Copy Number Gains	Copy Number Losses	Gene	Chromosome Coordinates	cDNA Variant	Exon	AA Change	CCF
1	Unmutated	1q31.3-q42.12	1q42.12-qter	*ATM*	11:108141998	c.2942G>C	20	p.R981P	1
	V3-48_J4	5	3pter-p25.3	*KMT2D*	12:49418631	c.15883G>C	49	p.G5295R	0.024
		7pter-p15.3	8p	*U2AF1*	21:44524456	c.101C>T	2	p.S34F	0.656
		8q21.3-qter	9pter-p13.1	*KDR*	4:55980364	c.727G>C	6	p.V243L	0.702
		9q21.11-q31.3	11q22.1-q23.3						
		16	15q13.1-q21.2						
		18q21.33	17pter-p13.2						
2	Unknown	2pter-p13.3	8pter-p11.1	*XPO1*	2:61719472	c.1711G>A	15	p.E571K	1
		8q13.3-q24.12	9pter-p21.3	*BTK*	X:100611164	c.1442G>C	15	p.C481S	0.412
		8q24.21-q24.3	11q22.3-q23.1	*ARID1B*	6:157469892	c.2687delT	9	p.L896Rfs*18	0.808
			13q14.2	*JAK3*	19:17943381	c.2627A>C	19	p.K876T	0.302
3	Unmutated	Trisomy 12	None	*XPO1*	2:61719472	c.1711G>A	15	p.E571K	0.504
	V3-21_J6			*KMT2D*	12:49420075	c.15674G>A	48	p.R5225H	0.168
				KMT2D	12:49434307	c.7246C>T	31	p.Q2416*	0.156
				PLCG2	16:81973594	c.3417_3419del AGA	30	p.E1139del	0.242
				PLCG2	16:81953154	c.2120C>T	20	p.S707F	0.058
				MED12	X:70339214	c.100-6_103del CCTCAGGATG	20	p.X34_splice	0.414
				TSHR	14:81609661	c.1259T>C	10	p.V420A	0.450
				PDGFRA	4:55140721	c.1582G>C	11	p.A528P	0.526
4	Mutated	Trisomy 12	9p21	*TP53*	17:7577538	c.743G>A	7	p.R248Q	0.996
	V3-11_J2	21	14q24-q32	*BTK*[#]	X:100611164	c.1441T>A	15	p.C481S	0.060
			17p12-p13	*BTK*[#]	X:100611165	c.1442G>C	15	p.C481S	0.566
			17q22	*BIRC3*	11:102207661	c.1644dupG	10	p.R549Afs*10	0.654
			17q25.3	*KMT2D*	12:49424471	c.13751dupC	41	p.V4585Sfs*21	0.092
				MED12	X:70339719	c.388G>T	3	p.A130S	0.624
				ARID4B	1:235344997	c.3237A>C	20	p.Q1079H	0.124
				BACH2	6:90642269	c.2384G>A	7	p.R795K	0.322
				FBXW7	4:153249384	c.1394G>T	9	p.R465L	0.654
				ATRX	X:76952086	c.349A>T	5	p.T117S	0.644
5	Unmutated	Trisomy 12	3p	*TP53*	17:7577551	c.712_729del TGTAACAGTTC CTGCATG	7	p.C238_M243del	0.182
	V4-39_J4		17p	*BTK*	X:100611163	c.1442_1443 delinsCT	15	p.C481S	0.184
			20q11-q12	*NOTCH1*	9:139390648	c.7541_7542 delCT	34	p.P2514Rfs*4	0.374
				BCL2	18:60985803	c.97G>A	2	p.G33R	0.210
				KMT2C	7:151891106	c.4648A>G	31	p.I1550V	0.244
				KMT2C	7:151884377	c.4962_4977del TCTCTACACCA ATATT	33	p.L1655Ifs*5	0.208
				PTPN11	12:112888166	c.182A>C	3	p.D61A	0.184
				SP140	2:231155209	c.1756_1757dup AA	19	p.A587Rfs*7	0.134
6	Unmutated	2pter-p14	1p22.2-p21.3	*SF3B1*	2:198266831	c.2101G>T	15	p.V701F	0.794
	V1-69_J4	7q21.11-qter	2q22.1-q22.3	*PLCG2*	16:81973603	c.3420T>A	30	p.D1140E	0.440
		8q21.3-qter	4q34.3-qter	*U2AF1*	21:44514801	c.446A>T	6	p.D149V	0.814
		13q22.3-q34	6q16.3-q26	*CTCF*	16:67671599	c.2008A>G	12	p.I670V	0.744
		16q23.3-q24.2	8pter-11.21						
		(*PLCG2*)	9pter-q21.1						
			11q13.5-q23.3						

			13q14.2-q14.3						
7	Unmutated	None	6p22.3-p22.1	*BRAF*	7:140453132	c.1803A>T	15	p.K601N	0.202
	V4-34_J6		9p21.3	*PLCG2*	16:81973614	c.3431A>G	30	p.D1144G	0.186
				MED12	X:70338701	c.97G>A	1	p.E33K	0.247
				POT1	7:124532332	c.112A>T	6	p.S38C	0.240
				MGA	15:41961674	c.584_601del ACTCTATGCAT CGTTACC	2	p.H195_Y200del	0.242
8	Unknown	None	None	*BTK*	X:100611165	c.1441T>C	15	p.C481R	0.160
9	Unmutated	None	*NOTCH1* Structural Variant	None	N/A	N/A	N/A	N/A	N/A
	V4-39_J4		(Exon 34 Deletion)						

Abbreviations: CLL = chronic lymphocytic leukemia, IGHV = immunoglobulin heavy chain gene variable region, *BTK* = Bruton's tyrosine kinase gene, *PLCG2* = phospholipase C gamma 2 gene, cDNA = complementary DNA, AA = amino acid, CCF = cancer cell fraction, N/A = not applicable.

[#]The *BTK* exon 15 mutations occur in *trans* (i.e. on different alleles).

Table S3. Molecular features of CLL patients at the time of clinical progression on pirtobrutinib.

ID	IGHV Mutation Status	Copy Number Gains	Copy Number Losses	Gene	Chromosome Coordinates	cDNA Variant	Exon	AA Change	CCF
1	Unmutated	7pter-p15.3	3pter-p25.3	*ATM*	11:108141998	c.2942G>C	20	p.R981P	0.398
	V3-48_J4	8q24.21	9p22.1-p13.1	*KMT2D*	12:49418631	c.15883G>C	49	p.G5295R	0.032
		18q21.33	11q22.1-q23.3	*U2AF1*	21:44524456	c.101C>T	2	p.S34F	0.318
				KDR	4:55980364	c.727G>C	6	p.V243L	0.298
				BTK	X:100611875	c.1246G>C	14	p.V416L	0.132
2	Unknown	2pter-p14	1q23.2-q23.3	*XPO1*	2:61719472	c.1711G>A	15	p.E571K	1
		8q13.3-q24.12	8pter-p11.1	*BTK*	X:100611164	c.1442G>C	15	p.C481S	0.872
		8q24.21-qter	8q11.21-q13.3	*BTK*	X:100611811	c.1310T>G	14	p.M437R	0.584
		17q21.33-q25	8q24.12-q24.13	*ARID1B*	6:157469892	c.2687delT	9	p.L896Rfs*18	0.754
			9pter-p21.3	*BIRC3*	11:102207817	c.1799G>C	10	p.R600P	0.106
			11q22.3-q23.3						
			13q14.2-q14.3						
3	Unmutated	Trisomy 12	None	*XPO1*	2:61719472	c.1711G>A	15	p.E571K	0.600
	V3-21_J6			*KMT2D*	12:49420075	c.15674G>A	48	p.R5225H	0.094
				KMT2D	12:49434307	c.7246C>T	31	p.Q2416*	0.250
				PLCG2	16:81973594	c.3417_3419delAGA	30	p.E1139del	0.280
				MED12	X:70339214	c.100-6_103delCCTCAGGATG	20	p.X34_splice	0.580
				TSHR	14:81609661	c.1259T>C	10	p.V420A	0.642
				PDGFRA	4:55140721	c.1582G>C	11	p.A528P	0.616
				BTK	X:100609666	c.1583T>G	16	p.L528W	0.298
4	Mutated	Trisomy 12	9p21.3-p21.1	*TP53*	17:7577538	c.743G>A	7	p.R248Q	1
	V3-11_J2	21	9q (CN-LOH)	*BTK*[#]	X:100611164	c.1441T>A	15	p.C481S	0.036
			14q23.2-q32.33	*BTK*[#]	X:100611165	c.1442G>C	15	p.C481S	0.136
			17p13.1-p12	*BTK*	X:100609666	c.1583T>G	16	p.L528W	0.578
			17q22	*BIRC3*	11:102207661	c.1644dupG	10	p.R549Afs*10	0.782
			17q24.3-q25.3	*MED12*	X:70339719	c.388G>T	3	p.A130S	0.700
				BACH2	6:90642269	c.2384G>A	7	p.R795K	0.160
				FBXW7	4:153249384	c.1394G>T	9	p.R465L	0.760
				ATRX	X:76952086	c.349A>T	5	p.T117S	0.724
				SETD5	3:9482357	c.785A>G	8	p.N262S	0.384
5	Unmutated	Trisomy 12	3pter-p11.2	*TP53*	17:7577551	c.712_729delTGTAACAGTTCCTGCATG	7	p.C238_M243del	0.370
	V4-39_J4		13q14.2-q14.3	*BTK*	X:100611185	c.1421C>T	15	p.T474I	0.334
			17pter-p11.2	*BTK*	X:100609666	c.1583T>G	16	p.L528W	0.288
			20q11.2-q13.12	*NOTCH1*	9:139390648	c.7541_7542delCT	34	p.P2514Rfs*4	0.626
				NOTCH1	9:139390861	c.7330C>T	34	p.Q2444*	0.338
				BCL2	18:60985803	c.97G>A	2	p.G33R	0.748
				KMT2C	7:151891106	c.4648A>G	31	p.I1550V	0.568
				PTPN11	12:112888166	c.182A>C	3	p.D61A	0.270
				SP140	2:231155209	c.1756_1757dupAA	19	p.A587Rfs*7	0.194
				DTX1	12:113515575	c.606_607delinsTT	2	p.Q203*	0.190
				HIST1H2BC	6:26124111	c.22G>A	1	p.A8T	0.308
				MGA	15:41991298	c.2130_2134delinsA	5	p.I711Kfs*3	0.294
				MGA	15:42041800	c.5995G>T	17	p.E1999*	0.288
				RAD50	5:131973787	c.3490G>C	23	p.E1164Q	0.294
				SPEN	1:16256243	c.3508C>T	11	p.R1170*	0.270
6	Unmutated	13q34 (*IRS2*)	4q35.2	*SF3B1*	2:198266831	c.2101G>T	15	p.V701F	0.200
	V1-69_J4	16q23.3 (*PLCG2*)	9pter-q21.1	*PLCG2*	16:81973603	c.3420T>A	30	p.D1140E	0.062

		16q24.1 (*IRF8*)		*U2AF1*	21:44514801	c.446A>T	6	p.D149V	0.176
				CTCF	16:67671599	c.2008A>G	12	p.I670V	0.220
				PHF6	X:133549136	c.820C>T	8	p.R274*	0.021
7	Unmutated	*RBM34* - *ARID4B* rearrangement	7p11.2-q11.23	*BRAF*	7:140453132	c.1803A>T	15	p.K601N	0.732
	V4-34_J6	*RBM34* (Ex1-3)	9p21.3	*PLCG2*	16:81973614	c.3431A>G	30	p.D1144G	0.724
		ARID4B (Ex 23-24)	10q24.32-q24.33	*MED12*	X:70338701	c.97G>A	1	p.E33K	0.406
			19p13.3-p11	*POT1*	7:124532332	c.112A>T	6	p.S38C	1
			19q13.1-q13.43	*MGA*	15:41961674	c.584_601del ACTCTATGCA TCGTTACC	2	p.H195_Y200del	0.746
			22q11.1-q13.31						
8	Unknown	12p	3pter-p21.31	*TP53*	17:7578221	c.626_627 delGA	6	p.R209Kfs*6	0.890
		14q32.32	10p11.23-p11.1	*TP53*	17:7577100	c.838A>G	8	p.R280G	0.914
			14q12-q22.3	*SF3B1*	2:198267360	c.1997A>C	14	p.K666T	0.910
			14q23.2-q24.2	*BTK*	X:100611165	c.1441T>C	15	p.C481R	0.953
			14q31.3-q32.31	*BTK*	X:100611185	c.1421C>T	15	p.T474I	0.944
			14q32.33	*BCL2*	18:60985514	c.386G>A	2	p.R129H	0.980
				IRF4	6:394946	c.342C>A	3	p.S114R	0.928
				SETD2	3:47158137	c.4562T>C	4	p.L1521P	1
				ACTG1	17:79478647	c.367_368 delAT	4	p.M123Vfs*2	0.906
9	Unmutated	8q13.2-q24.3	*NOTCH1* Structural Variant	*TP53*	17:7579561	c.106_125delC CGTCCCAAG CAATGGATGA	4	p.P36Ffs*9	0.690
	V4-39_J4	Trisomy 12	(Exon 34 Deletion)	*SF3B1*	2:198265579	c.2578G>A	18	p.E860K	0.542
			2q23.3-q24.3	*BTK*	X:100609666	c.1583T>G	16	p.L528W	0.256
			2q36.3-q37.1	*DDX3X*	X:41203641	c.1015_1018 delinsC	10	p.D339_F340 delinsL	0.519
			4p16.3-p15.1	*IGF1R*	15:99472883	c.2879G>T	14	p.R960I	0.854
			4q12-q13.2	*SETD1B*	12:122263112	c.5048G>C	13	p.S1683T	0.318
			6	*BRCA2*	13:32972596	c.9946G>C	27	p.E3316Q	0.626
			8pter-q11.1						
			8q11.23-q13.2						
			9						
			13q14.2-q14.3						
			15q11.2-q21.3						
			15q24.1-qter						
			17pter-p11.2						
			Xp22.33						

Abbreviations: CLL = chronic lymphocytic leukemia, IGHV = immunoglobulin heavy chain gene variable region, CN-LOH = copy neutral loss of heterozygosity, *BTK* = Bruton's tyrosine kinase gene, *PLCG2* = phospholipase C gamma 2 gene, cDNA = complementary DNA, AA = amino acid, CCF = cancer cell fraction

[#]The *BTK* exon 15 mutations occur in *trans* (i.e. on different alleles).

Table S4. Single cell DNA sequencing metrics.

Sample	Cell numbers	Reads (Million)	Reads per cell	Reads per amplicon per cell
ID3 Pre-treatment	3,048	458.04	11,586	42
ID3 On-treatment relapse	4,748	65.09	7,981	29
ID4 Pre-treatment	896	34.97	22,717	82
ID4 On-treatment relapse	6,013	65.89	6,554	23

Table S5. Pre-pirtobrutinib molecular features of CLL patients with on-treatment response to pirtobrutinib used for CITE-seq analyses.

ID	IGHV Mutation Status	Copy Number Gains	Copy Number Losses	Gene	Chromosome Coordinates	cDNA Variant	Exon	AA Change	CCF
ID 10	Unmutated	None	6q14.1-q22.32	*FBXW7*	4:153249391	c.1386delC	9	p.T463Lfs*35	0.522
	V1-46_J6		13q14.2q14.3	*BCL11B*	14:99723928	c.307C>T	2	p.R103C	0.540
				MGA	15:42021440	c.3736C>T	11	p.R1246*	0.586
ID 11	Unmutated	None	13q14.2-q14.3	*TP53*	17:7578221	c.626_627delGA	6	p.R209Kfs*6	0.088
	V3-21_J4		17p13.3-p12	*TP53*	17:7577544	c.737T>C	7	p.M246T	0.074
				TP53	17:7577108	c.830G>T	8	p.C277F	0.038
				BIRC3	11:102207675	c.1663_1666del AGAA	10	p.R555Hfs*12	0.248
				JAK2	9:5080684	c.2434+1G>T	18	p.X812_splice	0.584
				KRAS[#]	12:25398284	c.35G>A	2	p.G12D	0.100
				KRAS[#]	12:25398281	c.38G>A	2	p.G13D	0.070
				NOTCH1	9:139390648	c.7541_7542del CT	34	p.P2514Rfs*4	0.512
				TBL1XR1	3:176755936	c.1072G>T	12	p.D358Y	0.580

Abbreviations: CLL = chronic lymphocytic leukemia, IGHV = immunoglobulin heavy chain gene variable region, cDNA = complementary DNA, AA = amino acid, CCF = cancer cell fraction, N/A = not applicable.

[#]The *KRAS* exon 2 mutations occur in *trans* (i.e. on different alleles).

Table S6. Gene targets covered by the MSK-IMPACT Heme/HemePACT targeted next-generation sequencing 576-gene panel.

ABL1	*CD28*	*FGF19*	*IRF4*	*NKX2-1*	*RPTOR*	*TRAF5*	*GREM1*	*PPP6C*
ACTG1	*CD58*	*FGF3*	*IRF8*	*NOTCH1*	*RRAGC*	*TSC1*	*H3F3A*	*PRDM14*
AKT1	*CD79A*	*FGF4*	*IRS2*	*NOTCH2*	*RTEL1*	*TSC2*	*H3F3B*	*PREX2*
AKT2	*CD79B*	*FGFR1*	*JAK1*	*NOTCH3*	*RUNX1*	*TSHR*	*H3F3C*	*PRKCI*
AKT3	*CDC73*	*FGFR2*	*JAK2*	*NOTCH4*	*RUNX1T1*	*TYK2*	*HIST1H3A*	*PRKD1*
ALK	*CDH1*	*FGFR3*	*JAK3*	*NPM1*	*SAMHD1*	*U2AF1*	*HIST1H3C*	*PTP4A1*
ALOX12B	*CDK12*	*FGFR4*	*JARID2*	*NRAS*	*SDHA*	*U2AF2*	*HIST1H3D*	*PTPRD*
AMER1	*CDK4*	*FLCN*	*JUN*	*NSD1*	*SDHB*	*UBR5*	*HIST1H3E*	*PTPRS*
APC	*CDK6*	*FLT1*	*KDM5A*	*NT5C2*	*SDHC*	*VAV1*	*HIST1H3F*	*PTPRT*
AR	*CDK8*	*FLT3*	*KDM5C*	*NTRK1*	*SDHD*	*VAV2*	*HIST1H3H*	*RAB35*
ARAF	*CDKN1B*	*FLT4*	*KDM6A*	*NTRK2*	*SETBP1*	*VHL*	*HIST1H3I*	*RAC1*
ARHGEF28	*CDKN2A*	*FOXL2*	*KDR*	*NTRK3*	*SETD1A*	*WHSC1*	*HIST1H3J*	*RAC2*
ARID1A	*CDKN2B*	*FOXO1*	*KEAP1*	*P2RY8*	*SETD1B*	*WT1*	*HIST2H3C*	*RASA1*
ARID1B	*CDKN2C*	*FOXP1*	*KIT*	*PAK7*	*SETD2*	*XBP1*	*HIST2H3D*	*RBM10*
ARID2	*CEBPA*	*FURIN*	*KMT2A*	*PALB2*	*SETD3*	*XPO1*	*HIST3H3*	*RECQL*
ARID3A	*CHEK1*	*FYN*	*KMT2B*	*PARP1*	*SETD4*	*ZRSR2*	*HLA-B*	*RECQL4*
ARID3B	*CHEK2*	*GATA1*	*KMT2C*	*PAX5*	*SETD5*	*ACVR1*	*HOXB13*	*RFWD2*
ARID3C	*CIC*	*GATA2*	*KMT2D*	*PBRM1*	*SETD6*	*AGO2*	*ICOSLG*	*RHEB*
ARID4A	*CIITA*	*GATA3*	*KMT5A*	*PCBP1*	*SETD7*	*ANKRD11*	*IFNGR1*	*RIT1*
ARID4B	*CRBN*	*GNA11*	*KRAS*	*PDCD1*	*SETDB1*	*AXIN2*	*IL10*	*RPS6KA4*
ARID5A	*CREBBP*	*GNA12*	*KSR2*	*PDGFRA*	*SETDB2*	*BABAM1*	*INHA*	*RPS6KB2*
ARID5B	*CRKL*	*GNA13*	*LCK*	*PDGFRB*	*SF3B1*	*BBC3*	*INHBA*	*RRAS*
ASXL1	*CRLF2*	*GNAQ*	*LMO1*	*PDPK1*	*SGK1*	*BCL2L1*	*INPP4A*	*RRAS2*
ASXL2	*CSF1R*	*GNAS*	*LTB*	*PDS5B*	*SH2B3*	*BCL2L11*	*INPPL1*	*RXRA*
ATM	*CSF3R*	*GNB1*	*MALT1*	*PHF6*	*SMAD2*	*BMPR1A*	*INSR*	*RYBP*
ATP6AP1	*CTCF*	*GRIN2A*	*MAP2K1*	*PIGA*	*SMAD4*	*CARM1*	*IRS1*	*SDHAF2*
ATP6V1B2	*CTNNB1*	*GSK3B*	*MAP2K2*	*PIK3C2G*	*SMARCA4*	*CD276*	*KLF4*	*SESN1*
ATR	*CUX1*	*GTF2I*	*MAP2K4*	*PIK3C3*	*SMARCB1*	*CDC42*	*KNSTRN*	*SESN2*
ATRX	*CXCR4*	*HDAC1*	*MAP3K1*	*PIK3CA*	*SMARCD1*	*CDKN1A*	*LATS1*	*SESN3*
ATXN2	*CYLD*	*HDAC4*	*MAP3K13*	*PIK3CG*	*SMC1A*	*CENPA*	*LATS2*	*SH2D1A*
AURKA	*DAXX*	*HDAC7*	*MAP3K14*	*PIK3R1*	*SMC3*	*CSDE1*	*LYN*	*SHOC2*
AURKB	*DDR2*	*HGF*	*MAPK1*	*PIK3R2*	*SMG1*	*CTLA4*	*MAPKAP1*	*SHQ1*
AXIN1	*DDX3X*	*HIF1A*	*MAPK3*	*PIM1*	*SMO*	*CUL3*	*MAX*	*SLX4*
AXL	*DIS3*	*HIST1H1B*	*MCL1*	*PLCG1*	*SOCS1*	*CYSLTR2*	*MDC1*	*SMAD3*
B2M	*DNMT3A*	*HIST1H1C*	*MDM2*	***PLCG2***	*SOX2*	*DCUN1D1*	*MLL*	*SMYD3*
BACH2	*DOT1L*	*HIST1H1D*	*MDM4*	*PMS2*	*SP140*	*DICER1*	*MSH3*	*SOS1*
BAP1	*DTX1*	*HIST1H1E*	*MED12*	*PNRC1*	*SPEN*	*DNAJB1*	*MSI1*	*SOX17*
BARD1	*DUSP22*	*HIST1H2AC*	*MEF2B*	*POT1*	*SPOP*	*DNMT1*	*MSI2*	*SOX9*
BCL10	*EED*	*HIST1H2AG*	*MEN1*	*PPP2R1A*	*SRC*	*DNMT3B*	*MST1*	*SPRED1*
BCL11B	*EGFR*	*HIST1H2AL*	*MET*	*PRDM1*	*SRSF2*	*DROSHA*	*MST1R*	*STK19*
BCL2	*EGR1*	*HIST1H2AM*	*MGA*	*PRKAR1A*	*STAG1*	*DUSP4*	*MYOD1*	*STK40*
BCL6	*EP300*	*HIST1H2BC*	*MGAM*	*PTCH1*	*STAG2*	*E2F3*	*NCOA3*	*TAP1*
BCOR	*EP400*	*HIST1H2BD*	*MITF*	*PTEN*	*STAT3*	*EGFL7*	*NEGR1*	*TAP2*
BCORL1	*EPHA3*	*HIST1H2BG*	*MLH1*	*PTPN1*	*STAT5A*	*EIF1AX*	*NFKBIA*	*TCEB1*
BCR	*EPHA5*	*HIST1H2BJ*	*MOB3B*	*PTPN11*	*STAT5B*	*EIF4A2*	*NKX3-1*	*TCF3*
BIRC3	*EPHA7*	*HIST1H2BK*	*MPEG1*	*PTPN2*	*STAT6*	*EIF4E*	*NTHL1*	*TCF7L2*
BLM	*EPHB1*	*HIST1H2BO*	*MPL*	*RAD21*	*STK11*	*ELF3*	*NUF2*	*TEK*
BRAF	*ERBB2*	*HIST1H3B*	*MRE11A*	*RAD50*	*SUFU*	*EPAS1*	*NUP93*	*TGFBR1*
BRCA1	*ERBB3*	*HIST1H3G*	*MSH2*	*RAD51*	*SUZ12*	*EPCAM*	*PAK1*	*TMEM127*
BRCA2	*ERBB4*	*HLA-A*	*MSH6*	*RAD51B*	*SYK*	*ERCC2*	*PARK2*	*TMPRSS2*
BRD4	*ERG*	*HNF1A*	*MTOR*	*RAD51C*	*TBL1XR1*	*ERCC3*	*PDCD1LG2*	*TP53BP1*
BRIP1	*ESCO2*	*HRAS*	*MUTYH*	*RAD51D*	*TBX3*	*ERCC4*	*PGR*	*TRAF7*
BTG1	*ESR1*	*ID3*	*MYC*	*RAD52*	*TERT*	*ERCC5*	*PHOX2B*	*UPF1*
BTK	*ETNK1*	*IDH1*	*MYCL1*	*RAD54L*	*TET1*	*ERF*	*PIK3CB*	*VEGFA*
CALR	*ETV6*	*IDH2*	*MYCN*	*RAF1*	*TET2*	*ERRFI1*	*PIK3CD*	*VTCN1*
CARD11	*EZH2*	*IGF1*	*MYD88*	*RARA*	*TET3*	*ETV1*	*PIK3R3*	*WHSC1L1*
CASP8	*FAM46C*	*IGF1R*	*NBN*	*RB1*	*TGFBR2*	*EZH1*	*PLK2*	*WWTR1*
CBFB	*FANCA*	*IGF2*	*NCOR1*	*REL*	*TNFAIP3*	*FAM175A*	*PMAIP1*	*XIAP*
CBL	*FANCC*	*IKBKE*	*NCOR2*	*RET*	*TNFRSF14*	*FAM58A*	*PMS1*	*XRCC2*
CCND1	*FANCD2*	*IKZF1*	*NCSTN*	*RHOA*	*TOP1*	*FH*	*POLD1*	*YAP1*
CCND2	*FAS*	*IKZF3*	*NF1*	*RICTOR*	*TP53*	*FOXA1*	*POLE*	*YES1*
CCND3	*FAT1*	*IL7R*	*NF2*	*RNF43*	*TP63*	*FUBP1*	*PPARG*	*ZFHX3*

CCNE1	*FBXO11*	*INPP4B*	*NFE2*	*ROBO1*	*TRAF2*	*GLI1*	*PPM1D*	*ZBTB7A*
CD274	*FBXW7*	*IRF1*	*NFE2L2*	*ROS1*	*TRAF3*	*GPS2*	*PPP4R2*	*HIRA*

SUPPLEMENTARY REFERENCES

1. Durham BH, Getta B, Dietrich S, et al. Genomic analysis of hairy cell leukemia identifies novel recurrent genetic alterations. Blood 2017;130:1644-8.
2. Cheng DT, Mitchell TN, Zehir A, et al. Memorial Sloan Kettering-Integrated Mutation Profiling of Actionable Cancer Targets (MSK-IMPACT): A Hybridization Capture-Based Next-Generation Sequencing Clinical Assay for Solid Tumor Molecular Oncology. J Mol Diagn 2015;17:251-64.
3. Zehir A, Benayed R, Shah RH, et al. Mutational landscape of metastatic cancer revealed from prospective clinical sequencing of 10,000 patients. Nat Med 2017.
4. Ross DS, Zehir A, Cheng DT, et al. Next-Generation Assessment of Human Epidermal Growth Factor Receptor 2 (ERBB2) Amplification Status: Clinical Validation in the Context of a Hybrid Capture-Based, Comprehensive Solid Tumor Genomic Profiling Assay. J Mol Diagn 2017;19:244-54.
5. Carter SL, Cibulskis K, Helman E, et al. Absolute quantification of somatic DNA alterations in human cancer. Nat Biotechnol 2012;30:413-21.
6. Mason-Suares H, Kim W, Grimmett L, et al. Density matters: comparison of array platforms for detection of copy-number variation and copy-neutral abnormalities. Genet Med 2013;15:706-12.
7. Taylor J, Mi X, North K, et al. Single-cell genomics reveals the genetic and molecular bases for escape from mutational epistasis in myeloid neoplasms. Blood 2020;136:1477-86.
8. Dobin A, Davis CA, Schlesinger F, et al. STAR: ultrafast universal RNA-seq aligner. Bioinformatics 2013;29:15-21.
9. Liao Y, Smyth GK, Shi W. featureCounts: an efficient general purpose program for assigning sequence reads to genomic features. Bioinformatics 2014;30:923-30.
10. Law CW, Chen Y, Shi W, Smyth GK. voom: Precision weights unlock linear model analysis tools for RNA-seq read counts. Genome biology 2014;15:R29.
11. Pettersen EF, Goddard TD, Huang CC, et al. UCSF ChimeraX: Structure visualization for researchers, educators, and developers. Protein Sci 2021;30:70-82.
12. Bender AT, Gardberg A, Pereira A, et al. Ability of Bruton's Tyrosine Kinase Inhibitors to Sequester Y551 and Prevent Phosphorylation Determines Potency for Inhibition of Fc Receptor but not B-Cell Receptor Signaling. Mol Pharmacol 2017;91:208-19.
13. Reiff SD, Mantel R, Smith LL, et al. The BTK Inhibitor ARQ 531 Targets Ibrutinib-Resistant CLL and Richter Transformation. Cancer Discov 2018;8:1300-15.
14. Clark AJ, Tiwary P, Borrelli K, et al. Prediction of Protein-Ligand Binding Poses via a Combination of Induced Fit Docking and Metadynamics Simulations. J Chem Theory Comput 2016;12:2990-8.
15. Azam M, Seeliger MA, Gray NS, Kuriyan J, Daley GQ. Activation of tyrosine kinases by mutation of the gatekeeper threonine. Nat Struct Mol Biol 2008;15:1109-18.
16. Zheng GX, Terry JM, Belgrader P, et al. Massively parallel digital transcriptional profiling of single cells. Nat Commun 2017;8:14049.
17. Li B, Gould J, Yang Y, et al. Cumulus provides cloud-based data analysis for large-scale single-cell and single-nucleus RNA-seq. Nat Methods 2020;17:793-8.
18. Stoeckius M, Zheng S, Houck-Loomis B, et al. Cell Hashing with barcoded antibodies enables multiplexing and doublet detection for single cell genomics. Genome Biol 2018;19:224.
19. Hao Y, Hao S, Andersen-Nissen E, et al. Integrated analysis of multimodal single-cell data. bioRxiv 2020:2020.10.12.335331.
20. Welch JD, Kozareva V, Ferreira A, Vanderburg C, Martin C, Macosko EZ. Single-Cell Multi-omic Integration Compares and Contrasts Features of Brain Cell Identity. Cell 2019;177:1873-87 e17.